Using short-term postseismic displacements to infer the ambient deformation conditions of the upper mantle

Andrew M. Freed,[1] Greg Hirth,[2] and Mark D. Behn[3]

Received 31 May 2011; revised 23 November 2011; accepted 30 November 2011; published 31 January 2012.

[1] To interpret short-term postseismic surface displacements in the context of key ambient conditions (e.g., temperature, pressure, background strain rate, water content, creep mechanism), we combined steady state and transient flow into a single constitutive relation that can explain the response of a viscoelastic material to a change in stress. The flow law is then used to investigate mantle deformation beneath the Eastern California Shear Zone following the 1999 M7.1 Hector Mine earthquake. The flow law parameters are determined using finite element models of relaxation processes, constrained by surface displacement time series recorded by 55 continuous GPS stations for 7 years following the earthquake. Results suggest that postseismic flow following the Hector Mine earthquake occurs below a depth of ~50 km and is controlled by dislocation creep of wet olivine. Diffusion creep models can also explain the data, but require a grain size (3.5 mm) that is smaller than the inferred grain size (10–20 mm) based on the mantle conditions at these depths. In addition, laboratory flow laws predict dislocation creep would dominate at the stress/grain size conditions that provide the best fit to diffusion creep models. Model results suggest a transient creep phase that lasts ~1 year and has a viscosity ~10 times lower than subsequent steady state flow, in general agreement with laboratory observations. The postseismic response is best explained as occurring within a relatively hot upper mantle (e.g., 1200–1300°C at 50 km depth) with a long-term background mantle strain rate of 0.1–0.2 μstrain/yr, consistent with the observed surface strain rate. Long-term background shear stresses at the top of the mantle are ~4 MPa, then decrease with depth to a minimum of 0.1–0.2 MPa at 70 km depth before increasing slowly with depth due to the pressure dependence of viscosity. These conditions correspond to a background viscosity of 10^{21} Pa s within a thin mantle lid that decreases to $\sim 5 \times 10^{19}$ Pa s within the underlying asthenosphere. This study shows the utility of using short-term postseismic observations to infer long-term mantle conditions that are not readily observable by other means.

Citation: Freed, A. M., G. Hirth, and M. D. Behn (2012), Using short-term postseismic displacements to infer the ambient deformation conditions of the upper mantle, *J. Geophys. Res.*, *117*, B01409, doi:10.1029/2011JB008562.

1. Introduction

[2] Earthquakes can be used as large-scale rock deformation experiments to probe the rheology of the lower crust and upper mantle. Much like their laboratory counterparts on 1–10-mm sized specimens, these in situ rock-deformation experiments constrain how hot rocks flow in response to a change in stress under particular ambient conditions (e.g., temperature, pressure, water content). In the case of earthquakes, stress changes in the lower crust and upper mantle are induced by slip on a fault, and the resulting flow (postseismic relaxation) can be indirectly observed by the subsequent surface deformations. The pattern of postseismic surface displacements, along with displacement rate changes in the years after an earthquake, is a direct result of the coseismic loading and the viscoelastic rheology of the lower crustal and upper mantle [e.g., *Bürgmann and Dresen*, 2008]. Thus, with known coseismic stress changes and geodetically constrained postseismic displacements, one can infer the rheology of the lower crust and upper mantle and the ambient conditions that exist at depth. Furthermore, such in situ rock deformation experiments can be used to infer the dominant creep mechanism (i.e., diffusion creep versus dislocation creep), as well as (in the case of dislocation creep) the long-term background strain rate and absolute stress levels at the depths that respond to postseismic stress changes. Therefore, one can use short-term (years) postseismic observations to infer long-term (millennia) ambient conditions that are not readily measureable by other means.

[3] Several key conditions must be met to use postseismic observations to infer lower crustal and mantle rheology and

[1]Department of Earth and Atmospheric Sciences, Purdue University, West Lafayette, Indiana, USA.
[2]Geological Sciences, Brown University, Providence, Rhode Island, USA.
[3]Department of Geology and Geophysics, Woods Hole Oceanographic Institution, Woods Hole, Massachusetts, USA.

0148-0227/12/2011JB008562

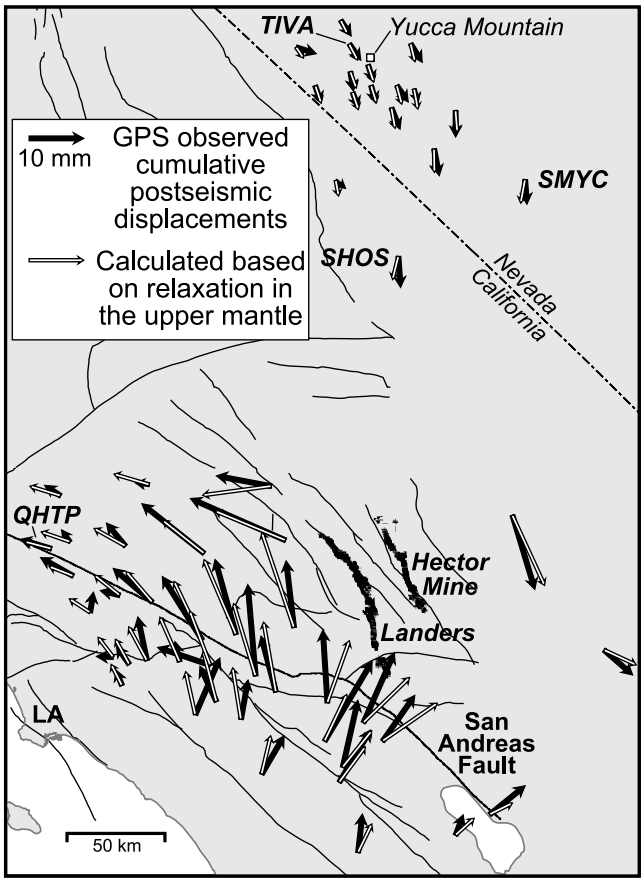

Figure 1. Cumulative GPS observed postseismic horizontal surface displacements (transient component) for the 7 year period following the 1999 Hector Mine earthquake compared to those calculated by a model of steady state dislocation creep of a wet olivine upper mantle. Stations within 50 km of the Hector Mine rupture surface have been excluded from this study to limit comparisons to stations where surface displacements are primarily due to mantle flow.

background ambient conditions. First, larger earthquakes, probably M7 or greater, are required to induce large enough stress changes in the lower crust and upper mantle to drive measureable postseismic relaxation at the surface [e.g., *Freed*, 2007; *Mahsas et al.*, 2008]. Second, the moment magnitude of the slip distribution of the earthquake must be well constrained. Third, postseismic observations need to be broad enough to discern the overall pattern of postseismic surface deformation (i.e., more than a simple transect of GPS stations across a rupture surface). Fourth, sufficient geodetic measurements as a function of time are required to ascertain displacement rate changes, especially in the first year after the earthquake. And fifth, a constitutive relationship must account for both the effects of ambient tectonic conditions on steady state creep and the transient creep that occurs immediately following the earthquake.

[4] Previous analyses considered the role of ambient stress conditions in conjunction with a stress-dependent power law rheology (dislocation creep) to explain observed postseismic displacement rate changes [e.g., *Freed and Bürgmann*, 2004; *Freed et al.*, 2006; *Hearn et al.*, 2009]. In general, such analyses require relatively small background stress levels (0.1 MPa or less) to explain fast early postseismic displacement rates that decrease rapidly after the first year. Low background stresses are required because the co-seismic stress change must be on order of the background stress in order for significant creep to occur. For example, models for postseismic relaxation following the 2002 Denali, Alaska earthquake, [*Freed et al.*, 2006] and the 1999 Izmit and Düzce earthquake ruptures [*Hearn et al.*, 2005, 2009] indicate background stress levels up to 10 times smaller than the magnitude of coseismic stress changes are needed for a power law rheology to explain observed postseismic rate changes.

[5] To explain early fast surface displacement rates, other studies considered the role of transient creep [*Pollitz*, 2003, 2005; *Hearn et al.*, 2009]. During transient creep, an initial phase of flow follows an imposed stress change at much higher strain rates than predicted from the steady state flow law [e.g., *Post*, 1977; *Chopra*, 1997]. Specifically, *Pollitz* [2003, 2005] and *Hearn et al.* [2009] employed a bi-viscous constitutive relation (Burgers model) for which a transient and a steady state viscosity are assumed. While these studies adequately simulate postseismic displacement rates, the generality of the rheological laws is limited because the inferred viscosity structure is not directly related to the ambient conditions.

[6] Laboratory experiments suggest, however, that both power law flow and transient creep are likely occurring immediately following a sudden stress change, such as an earthquake. This idea is supported by models of postseismic rate changes following the 1999 Hector Mines earthquake. Utilizing a longer postseismic time series (7 years) and many more GPS stations (especially far-field) than previous studies, *Freed et al.* [2010] showed that while dislocation creep of wet olivine can explain 7 year cumulative displacements (Figure 1), such a rheology cannot explain fast early postseismic surface displacement rates (Figure 2) without appealing to implausible background ambient conditions. An analysis that utilizes a power law rheology, but ignores a transient phase, will underestimate background stress levels, perhaps explaining the small background stress magnitudes inferred by previous power law studies [e.g., *Freed et al.*, 2006; *Hearn et al.*, 2009]. As pointed out by *Hearn et al.* [2009], a background stress of 0.1 MPa or less is likely incompatible with the occurrence of dislocation creep unless unusually large grain sizes (>100 mm) are present.

[7] In this paper we focus on the constitutive relationships that link the steady state and transient creep phases. We combine viscoelastic constitutive laws into a single relationship between strain rate and stress that explains the spatial and temporal characteristics of postseismic behavior as a function of the ambient environment. Specifically, we incorporate values of ambient parameters (e.g., temperature, grain size, and water content) appropriate for southern California into a generalized viscoelastic flow law. Flow law parameters are then constrained using a finite element model of postseismic relaxation following the 1999 M7.1 Hector Mine, California earthquake. Postseismic surface displacements measured by GPS following the Hector Mine earthquake are ideal to constrain such a model for several reasons. The broad coverage using more than 55 continuous GPS stations clearly illuminates the pattern of postseismic surface deformation (Figure 1) as well as displacement rate changes

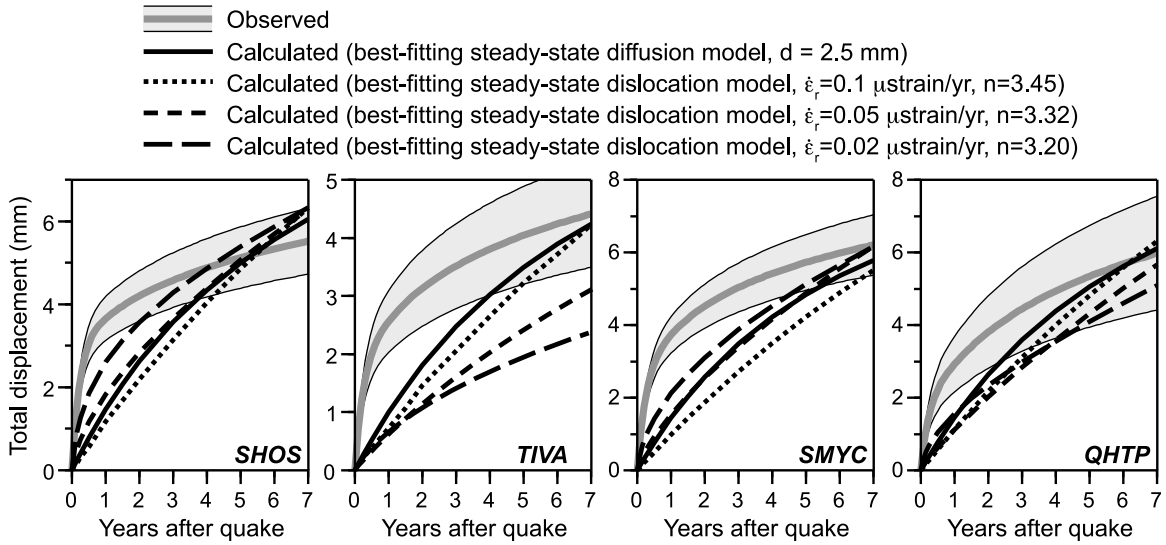

Figure 2. Comparison of observed versus calculated steady state displacement time series following the 1999 Hector Mine earthquake at 4 representative far-field locations. The observed time series are a functional representation based on a logarithmic fit (200 day decay time) to the transient component of GPS data after background secular, coseismic offsets, and annual and semiannual components are removed [*Freed et al.*, 2010]. Thin lines show 1σ error range. The calculated time series are based on the best fitting steady state diffusion and dislocation models (see text).

for more than 7 years after the earthquake (Figure 2). We focus on stations located more than 50 km away from the epicenter as *Freed et al.* [2007] demonstrated that viscoelastic relaxation in the mantle can only be isolated in far-field GPS data where contributions from afterslip and poroelastic rebound are unlikely. Our results show that the postseismic surface deformations are best explained by dislocation creep of wet olivine, with a transient creep phase that lasts ~1 year and has a viscosity ~10 times lower than subsequent steady state flow.

2. Coupling Transient and Steady-State Flow Laws

[8] To motivate the explicit accounting for transient creep in a flow law that also incorporates ambient parameters (e.g., temperature, back ground strain rate, grain size, and water content), we review the results of previous analyses that used only steady state flow laws [*Freed et al.*, 2010]. Steady state flow of the mantle is modeled using a power law relationship between stress and strain rate, $\dot{\varepsilon}$, for olivine [e.g., *Carter and Tsenn*, 1987; *Kirby and Kronenberg*, 1987; *Hirth and Kohlstedt*, 2003],

$$\dot{\varepsilon} = A\, d^{-p}\, C_{OH}^{r}\, \sigma^{n}\, e^{-(Q+PV)/RT} \tag{1}$$

where A is a prefactor ($MPa^{-n}\ s^{-1}$), d is grain size, p is the grain size exponent (0 for dislocation creep), C_{OH} is olivine water content (molar hydroxyl concentration, $H/10^6Si$), r is the water content exponent, σ is the differential stress, n is the stress exponent (1 for diffusion creep), Q is activation energy, P is pressure, V is activation volume, R is the universal gas constant, and T is absolute temperature. Utilizing this relationship, *Freed et al.* [2010] solved for the best fitting diffusion creep and dislocation creep models for the Hector Mine earthquake (Figure 2), the former being primarily a function of grain size and temperature, while the latter is primarily a function of background strain rate, stress exponent, and temperature. These results show that the assumption of steady state flow leads to an underprediction of early fast surface displacement rates, while overpredicting later rates (Figure 2). Several important features of these models are highlighted below.

[9] First, in the case of dislocation creep, lower assumed background strain rates result in greater displacement rate changes following the earthquake. This results from the stress-dependence ($n > 1$) of dislocation creep, which leads to lower background stress levels for lower background strain rates. If coseismic stress changes in the mantle are larger than the background stress levels, then viscoelastic relaxation rates are significantly influenced by the stress dependence of dislocation creep as coseismic stresses diminish. This stress dependence results in sharper curvature of the time series for the 0.02 μstrain/yr background strain rate case in Figure 2. In contrast, a higher background strain rate leads to background stresses significantly greater than the coseismic stress changes. In this case, the coseismic stress change does not greatly influence the overall creep rates, resulting in the flatter curvature of the time series for the 0.1 μstrain/yr background strain rate case in Figure 2.

[10] Second, while assuming a lower background strain rate leads to greater displacement rate changes, the far-field displacements are too small. Due to the lower background strain rate, the postseismic creep is concentrated in the shallow mantle directly beneath the rupture, leading to smaller wavelength postseismic surface deformation. This effect is seen in the time series for station TIVA, where cumulative displacements fall well short of those observed, and occurs at all of the stations in the Yucca Mountain region to the north and many far-field stations to the west. These results

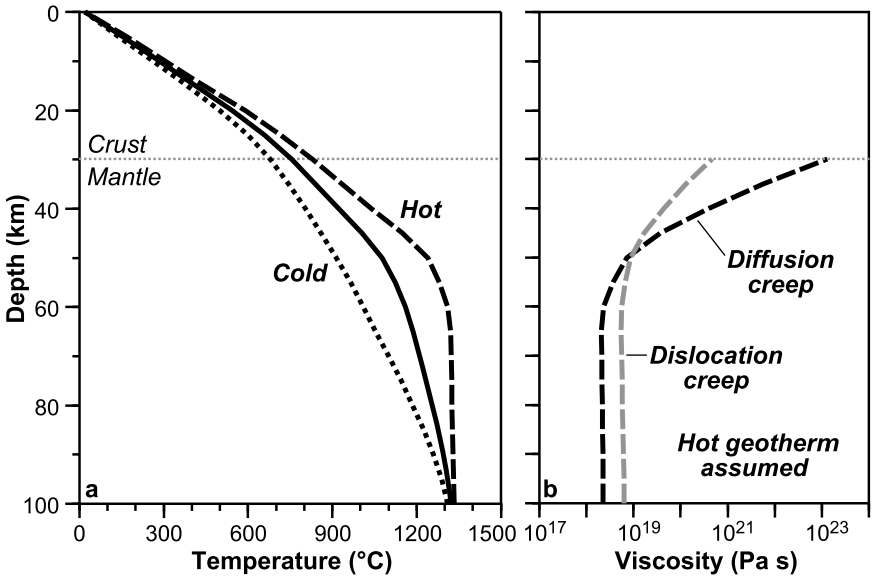

Figure 3. (a) Range of plausible thermal gradients used in this study based on variations of attenuation and shear velocities beneath the Mojave Desert [*Yang and Forsyth*, 2008]. (b) Comparison of the mantle viscosity structure from the best fitting steady state diffusion and dislocation creep models (Figure 2). Both models assume a hot geotherm, the diffusion model assumes a grain size of 0.25 mm, the dislocation model assumes a background strain rate of 0.1 μstrain/yr, other parameters as shown in Table 1.

highlight the trade-off between simulating higher rate changes versus broader surface deformation in dislocation models with varying background strain rate. Furthermore, we emphasize that none of these models can satisfy the observed time series.

[11] Third, the dislocation creep model that best fits the cumulative data leads to less curvature (rate changes) then the Newtonian (n = 1) diffusion case (Figure 2). This result is not intuitive, as one would expect power law (n > 1) models to lead to greater rate changes than Newtonian models. However, the best fitting dislocation creep model required a high background strain rate, leading to only modest changes in creep rate as the coseismic stress is relaxed. Furthermore, the activation energy for diffusion creep (Q = 335 kJ/mol) is lower than that for dislocation creep (Q = 480 kJ/mol) [*Hirth and Kohlstedt*, 2003], which leads to a different temperature dependence and associated viscosity as a function of depth. The background viscosity structures for the best fitting diffusion creep model and high background strain rate dislocation creep models are shown in Figure 3b. These models lead to similar 7 year cumulative surface displacements, but the diffusion creep model has lower viscosity at depth and therefore relaxes faster then the dislocation creep model (Figure 2). Had the diffusion creep and dislocation creep models led to the same viscosity structures, the high background strain rate dislocation model would have led to quicker rate changes because of its stress-dependence.

[12] The failure of steady state flows law to explain the post-Hector Mine time series implies that transient creep must be accounted for in a successful model of post-seismic creep. Laboratory experiments demonstrate that in response to a change in loading conditions, an initial transient phase marked by more rapid flow strain rates precedes a slower steady state response [e.g., *Carter and Kirby*, 1978; *Smith and Carpenter*, 1987; *Chopra*, 1997; *Gribb and Cooper*, 1998, 2000; *Cooper*, 2002]. Transient creep is thought to occur as the internal stress distribution and/or microstructure of the grains evolve in response to a change in the externally applied stress field [*Karato*, 2008]. Strain rate as a function of time for transient creep can be characterized by,

$$\dot{\varepsilon} = \dot{\varepsilon}_0 + (\dot{\varepsilon}_\infty - \dot{\varepsilon}_0)\left[1 - e^{-t/\tau}\right] \quad (2)$$

where $\dot{\varepsilon}_0$ is the initially high strain rate, $\dot{\varepsilon}_\infty$ is the steady state strain rate, t is time since the stress change, and τ is the transient relaxation time [e.g., *Karato*, 2008]. This can be reformulated in terms of a Burgers rheology,

$$\dot{\varepsilon} = \dot{\varepsilon}_\infty \left[1 - e^{-t/\tau} + \beta e^{-t/\tau}\right] \quad (3)$$

where $\beta = \dot{\varepsilon}_0/\dot{\varepsilon}_\infty$ is the ratio of the transient to the steady state strain rate, or equivalently, $\beta = \eta_\infty/\eta_0$, the ratio of the steady state to the transient viscosity. The latter definition for β is useful because laboratory results for transient creep are often reported in terms of relative viscosities. The relationship between transient creep and steady state creep can also be expressed using the Andrade model [e.g., *Gribb and Cooper*, 1998, 2000; *Cooper*, 2002].

[13] Although transient creep of wet olivine has not been systematically studied in detail, experiments show β of the order of 2–10 [*Carter and Ave Lallemant*, 1970; *Post*, 1977; *Mackwell et al.*, 1985; *Chopra*, 1997]. These experimental results suggest that τ is inversely proportional to the strain rate (proportional to viscosity) [*Post*, 1977; *Smith and Carpenter*, 1987]. For a Burgers rheology τ is often expressed as η/μ, where η is viscosity and μ is the shear modulus. Assuming a typical asthenosphere viscosity of 10^{19} Pa s and μ = 60 GPa results in a τ of 5 years. Thus, a transient

Table 1. Flow-Law Parameters

Symbol	Description	Value	Units
A_{diff}	Diffusion creep Prefactor	3.33×10^5 [a]	$MPa^{-1}\ s^{-1}$
r_{diff}	Diffusion creep water exponent	1	
p_{diff}	Diffusion creep grain-size exponent	3	
n_{diff}	Diffusion creep stress exponent	1	
Q_{diff}	Diffusion creep activation energy	335 ± 75	$kJ\ mol^{-1}$
V_{diff}	Diffusion creep activation volume	4 ± 4[b]	$cm^3\ mol^{-1}$
A_{disl}	Dislocation creep Prefactor	30[a]	$MPa^{-n}s^{-1}$
r_{disl}	Dislocation creep water exponent	1.2	
p_{disl}	Dislocation creep grain-size exponent	0	
n_{disl}	Dislocation creep stress exponent	3.5 ± 0.3	
Q_{disl}	Dislocation creep activation energy	480 ± 40	$kJ\ mol^{-1}$
V_{disl}	Dislocation creep activation volume	11 ± 5	$cm^3\ mol^{-1}$
σ_{ref}	Reference differential stress	100	MPa
P_{ref}	Reference pressure	300	GPa
T_{ref}	Reference temperature	1250	°C
R	Universal Gas Constant	8.31451	$J\ mol^{-1}\ K^{-1}$
β	Ratio of steady state to transition viscosity		
τ	Transition relaxation time		year

phase is expected to be active in the first few years after an earthquake.

[14] Biviscous Burgers rheologies have been used to explain fast early postseismic displacement rates in several studies. Following the 1999 M7.6 Izmit and M7.2 Düzce earthquake sequence, *Hearn et al.* [2009] found $\beta = 4$–10, consistent with the range inferred from the laboratory experiments. In contrast, *Pollitz* [2003, 2005] inferred a value of $\beta = 28$ in studies of postseismic displacements following the 1999 Hector Mine and 2002 M7.9 Denali, Alaska earthquakes. However, the Pollitz studies consisted of almost entirely of near-field GPS observations (within one rupture length) and did not consider the influence of shallow afterslip, which likely contributed significantly to rapid early displacement rates at those sites (as shown by *Hearn et al.* [2009]).

[15] We combine a biviscous constitutive relationship (3) with a steady state olivine flow law (1). In this way, we take advantage of laboratory observations that show the temperature- and stress-dependence of transient creep is similar to that of steady state creep [*Post*, 1977; *Smith and Carpenter*, 1987; *Chopra*, 1997; *Gribb and Cooper*, 1998, 2000; *Cooper*, 2002]. We combine equations (1) and (3) to yield,

$$\dot{\varepsilon} = A\, d^{-p}\, C_{OH}^{r}\, \sigma^{n}\, e^{-(Q+PV)/RT} \left[1 - e^{-t/\tau} + \beta e^{-t/\tau}\right] \qquad (4)$$

Equation (4) reverts to the steady state relationship for $\beta = 1$. This constitutive law allows us to simultaneously incorporate the effects of transient creep and ambient environmental conditions. In the following sections, we investigate the trade-offs between the transient creep (β and τ) and the ambient environment parameters (T, $\dot{\varepsilon}$, d, and C_{OH}).

3. Sensitivity of Mantle Viscosity to Uncertainties in Flow Law Parameters and Ambient Mantle Conditions

[16] A challenge of our analysis of post-seismic deformation is the large number of flow law parameters (and their uncertainties) required to describe mantle creep. In this section we examine the influence of the uncertainties in flow law parameters on viscosity to determine the parameter ranges that need to be considered. Since the temperature and stress dependence of transient and steady state viscosities are similar, we evaluate only the effects of uncertainty in the steady state flow law parameters. We cast the steady state flow law (3) in terms of the viscosity

$$\eta = \sigma / 2\,\dot{\varepsilon}. \qquad (5)$$

Combining (3) and (5) we can express viscosity in terms of stress:

$$\eta = \sigma^{1-n} e^{(Q+PV)/RT} / 2A d^{-p} C_{OH}^{r}, \qquad (6)$$

or in terms of strain rate:

$$\eta = \dot{\varepsilon}^{(1-n)/n} e^{(Q+PV)/nRT} / 2 \left(A d^{-p} C_{OH}^{r}\right)^{1/n}. \qquad (7)$$

Due to its abundance (with a volume fraction of 60–75%) and lower strength compared to other mantle minerals, olivine is believed to control upper mantle rheology [*Borch and Green*, 1987; *Handy*, 1990; *Karato and Wu*, 1993]. *Freed et al.* [2010] showed that dry olivine leads to too high a viscosity to explain the rapid flow in the mantle inferred to have occurred after the Hector Mine earthquake, and thus we consider only flow law parameters for diffusion creep and dislocation creep of wet olivine. Larger grain sizes and shear stresses favor dislocation creep; extrapolation of steady state flow laws suggests that this mechanism is dominant in the uppermost mantle [*Karato and Wu*, 1993; *Hirth and Kohlstedt*, 2003]. The dominance of dislocation creep is also supported by the observation of seismic anisotropy at depths above ~200 km, including beneath southern California [*Polet and Kanamori*, 2002]. Dislocation creep produces a lattice-preferred orientation, which results in seismic anisotropy. However, a weak shallow asthenosphere may be characterized by relatively low stresses, potentially promoting diffusion creep [*Karato and Wu*, 1993]. Thus, diffusion creep cannot be discounted.

[17] Flow law parameters and their uncertainties for wet olivine are taken from *Hirth and Kohlstedt* [2003] (Table 1). Uncertainties for water and grain size exponents were not reported by *Hirth and Kohlstedt* [2003]; a statistical study of several laboratory results by *Korenaga and Karato* [2008], including the Hirth and Kohlstedt data, shows the uncertainties of these exponents to be relatively small. We therefore assume the uncertainties of these exponents to be less influential on the viscosity calculation than the uncertainty in the absolute water content and grain size.

[18] As discussed by *Behn et al.* [2009], the uncertainty in the prefactor term, A, is often confused in the literature. The uncertainty in A covaries with the uncertainties of the other flow-law parameters. For our study this can be formulated:

$$A = A_{ref}\, \frac{\sigma_{ref}^{n_{ref}}\, e^{-\left(Q_{ref} + P_{ref} V_{ref}\right)/RT_{ref}}}{\sigma_{ref}^{n}\, e^{-\left(Q + P_{ref} V\right)/RT_{ref}}}, \qquad (8)$$

where A_{ref}, n_{ref}, Q_{ref}, and V_{ref} are the nominal flow-law parameters (either diffusion or dislocation creep); n, Q, and V are the assumed values for a candidate rheology, and σ_{ref}, P_{ref}, and T_{ref} are the reference conditions from which these

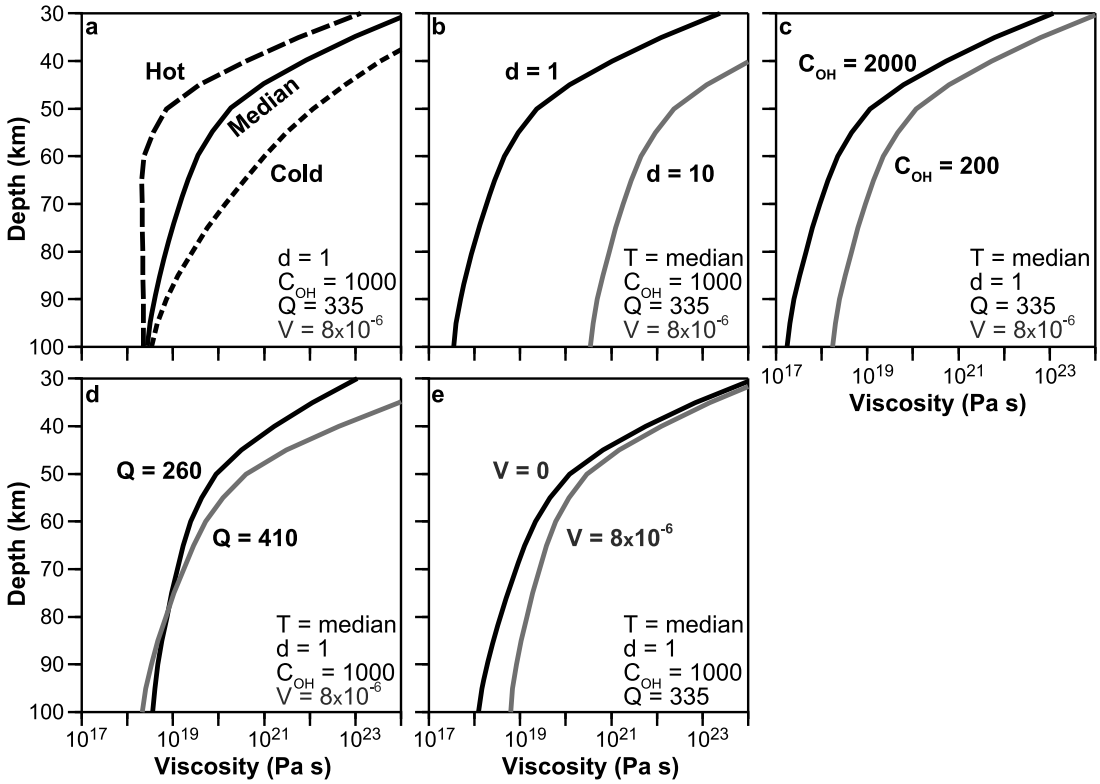

Figure 4. Sensitivities of variations of parameters to viscosity as a function of depth for diffusion creep of wet olivine: (a) thermal gradient (T), (b) grain size (mm), (c) water content (H/10^6 Si), (d) activation energy (kJ/mol), and (e) activation volume (cm^3/mol). Except for the parameter being varied in each panel, the calculation assumes the median value for all diffusion flow-law parameters (Table 1), A as calculated in equation (8), the median thermal gradient (Figure 3), d = 1 mm, C_{OH} = 1000 H/10^6 Si, and P = 3000 kg/m^3 × 10 m/s^2 × depth (m).

flow-law parameters were derived (Table 1). Following *Behn et al.* [2009], the nominal prefactor terms in Table 1 have been reduced by a factor of 3 compared to *Hirth and Kohlstedt* [2003] due to the re-calibration for water content in olivine [*Bell et al.*, 2003].

[19] We constructed hot, median, and cold geotherms (Figure 3) from a plausible range of thermal gradients in southern California based on variations of attenuation and shear velocities [*Yang and Forsyth*, 2008]. For reference, these geotherms are consistent with the observed heat flow range observed in the Mojave region (75–90 mW/m^2; http://smu.edu/geothermal/heatflow/heatflow.htm [*Lachenbruch*, 1978]). Resolvable postseismic relaxation of the mantle occurs only to a depth of ~100 km, regardless of viscosity, owing to the insignificance of coseismic stress changes below this depth. Thus, model results are not sensitive to temperatures below this depth [see also *Pollitz and Thatcher*, 2010]. Water content in the mantle beneath southern California is not well constrained. We assume a range of C_{OH} ranging from 200 H/10^6Si (relatively dry upper mantle) to 2000 H/10^6Si. Olivine water contents in this range have been measured in xenoliths from the nearby Basin and Range Provence and Colorado Plateau [*Li et al.*, 2008]. For reference, the water solubility of olivine at 2 GPa and 1300°C is ~7500 H/10^6Si (*Zhao et al.* [2004], corrected for calibration from *Bell et al.* [2003]).

[20] For diffusion creep we calculate viscosity variations as a function of depth (equation (7) with n = 1) using the hot and cold end-member geotherms with reference ambient conditions of d = 1 mm, C_{OH} = 1000 H/10^6 Si, $P = \rho gz$ based on a crustal density, ρ_c, of 2900 kg/m^3, a mantle density, ρ_m, of 3300 kg/m^3, and gravity, g = 9.8 m/s^2, with the median flow law parameters for diffusion creep of wet olivine listed in Table 1. Figure 4a shows that the depth-dependence of viscosity depends strongly on the assumed geotherm. This difference can be offset by, for example, assuming a smaller grain size for the colder geotherm model (which would result in a leftward shift of the dashed curve in Figure 4a). Nonetheless, for models with the same vertically integrated viscosity, the hot geotherm model (with larger grain size) leads to shallower flow with respect to the cold geotherm model (with a smaller grain size). This in turn leads to differences in the resulting pattern of surface deformation, which can then be used to constrain the most plausible geotherm.

[21] Using the median geotherm, Figures 4b–4e show how variations in grain size, water concentration, activation energy, and activation volume influence the calculated viscosity structure for diffusion creep. Of these, the influence of grain size on viscosity is most significant. In comparison to temperature and grain size, water concentration, activation energy, and activation volume have a much smaller influence on the viscosity structure, and thus we do not consider

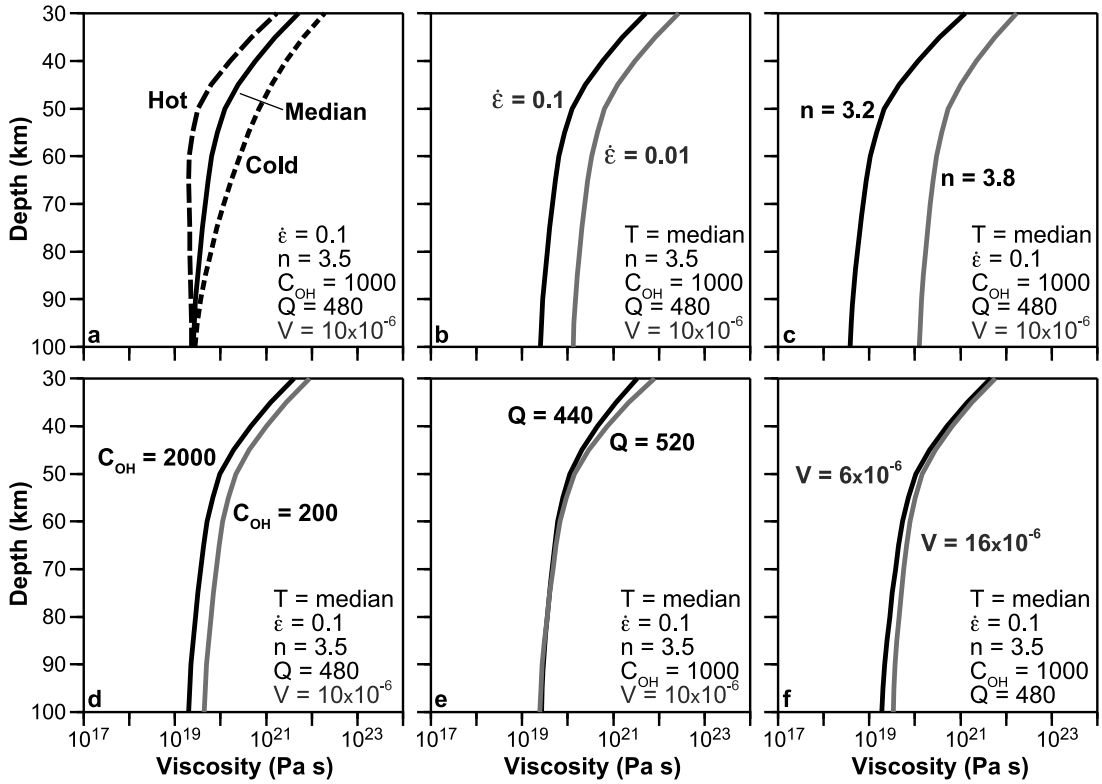

Figure 5. Sensitivities of variations of parameters to viscosity as a function of depth for dislocation creep of wet olivine: (a) thermal gradient (T), (b) background strain rate (μstrain/yr), (c) stress exponent, (d) water content (H/10^6 Si), (e) activation energy (kJ/mol), and (f) activation volume (cm^3/mol). Except for the parameter being varied in each panel, the calculation assumes the median value for all dislocation flow-law parameters (Table 1), A as calculated in equation (8), the median thermal gradient (Figure 3), $\dot{\varepsilon}$ = 0.1 μstrain/yr, C_{OH} = 1000 H/10^6 Si, and P = 3000 kg/m^3 × 10 m/s^2 × depth (m).

uncertainties in these parameters in our study. For example, variations in viscosity owing to realistic variations in water content (200–2000 H/10^6 Si) are approximately equivalent to variations associated with a change in temperature of ±40°C, only a fraction of the 300°C uncertainty in temperature at 50 km depth. Variations in viscosity due to the uncertainties in activation energy and activation volume on viscosity are even smaller.

[22] We repeat this sensitivity exercise for dislocation creep parameters using equation (7) with an assumed background strain rate of 0.1 μstrain/yr (measured surface strain rate in the Eastern California Shear Zone (ECSZ) where the Hector Mine earthquake occurred [*Savage et al.*, 2003]). Temperature, background strain rate, and the stress exponent have the strongest influence on the calculated viscosity structure (Figure 5). Most relevant for this study is the large effect of the stress exponent on viscosity (Figure 5c). Specifically, small uncertainties in the stress exponent (±0.3) result in large differences in viscosity, due the large extrapolation from the laboratory stress state (~100 MPa) to in situ conditions (~1 MPa).

4. Modeling Approach

[23] We use the ABAQUS (www.simulia.com/products/abaqus_fea.html) finite element framework of *Freed et al.* [2010] for the southwestern U.S. centered at the epicenter of the Hector Mine earthquake. This model simulates coseismic slip associated with both the 1992 M7.3 Landers [*Fialko*, 2004] and 1999 M7.1 Hector Mine [*Simons et al.*, 2002] earthquakes (verification of the coseismic models was discussed by *Freed et al.*, [2007]). Coseismic slip is simulated using constraint equations that define how the two sides of a fault (slit in the mesh) move relative to each other. Required simplifications of fault geometry and coseismic slip lead to some near-field misfit to GPS data. However, these misfits do not significantly influence calculated stresses in the mantle where postseismic flow occurs because the local stress concentrations associated with the small scale slip structure decrease with depth through the intervening crust, which acts as a low-pass filter (see Figures S1–S3 in the auxiliary material).[1] We utilize the same seismic velocity based elastic structure as these coseismic studies. As the Landers and Hector Mine earthquakes occurred in relatively close proximity (25 km distance) and postseismic relaxation from the Landers event was ongoing following the Hector Mine event, both earthquakes were considered in the simulations. Following *Freed et al.* [2010], we utilize velocity boundary conditions to generate a background strain rate field across the ECSZ region. These conditions are applied until steady state stress levels are achieved in the mantle

[1]Auxiliary materials are available in the HTML. doi:10.1029/2011JB008562.

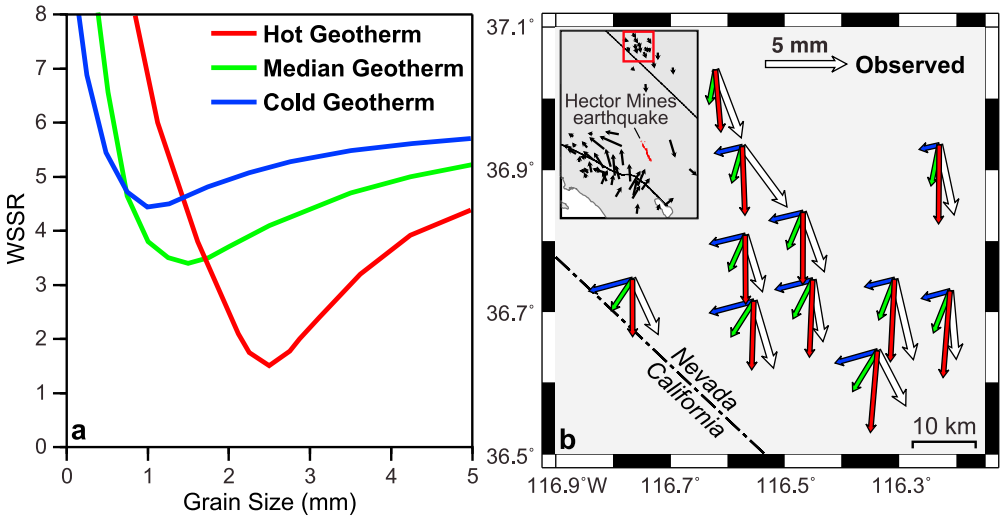

Figure 6. (a) Misfit (WSSR) of steady state diffusion creep models to 7 year cumulative displacements as a function of the assumed thermal gradient (Figure 3) and grain size (other diffusion parameters as listed in Table 1). (b) Influence of the assumed thermal gradient on the azimuth of cumulative postseismic displacements for the best fitting steady state models for each assumed geotherm. Shown are stations in the far-field region 200 km to the north of the Hector Mine epicenter (see inset).

(this portion of the run is only utilized for dislocation creep runs). After ambient strain rate and stresses are calculated, coseismic slip from the Landers earthquake is applied and the system is allowed to relax for 7 years. Finally, coseismic slip from the Hector Mine earthquake is applied and the system is allowed to relax for an additional 7 years. It is this last 7 year interval where surface displacements are extracted from the model and compared to the GPS time series.

[24] Our approach to testing candidate rheologies is to use a weighted sum of squared residuals (*wssr*) of the form,

$$wssr = sqrt\left[(1/m)\sum (L/150)(x_o - x_c)^2/\sigma^2\right] \qquad (9)$$

where x_o and x_c are the observed and calculated displacements (the N-S and E-W components at each GPS station are considered separate observations), σ is the observational error, m is the total number of observations, and L is the distance (in km) of the GPS station from the Hector Mine epicenter. We removed data from stations within 50 km of the Hector Mine rupture surface from the *wssr*, as postseismic displacements from these stations contain crustal components (afterslip, lower crustal flow, and/or poroelastic rebound). *Freed et al.* [2007] concluded that only stations beyond 150 km from the epicenter have displacements that are purely associated with mantle flow, while closer stations may record some small crustal postseismic component. To ensure that our results are not significantly biased by crustal contributions, we added a $L/150$ weighting term (set to not exceed 1) to linearly diminish the influence of displacements from stations between 50 and 150 km from the epicenter. This weighting term only has a slight influence on model results (see Figure S4).

[25] We use a forward modeling approach to find the rheology (flow law parameters) and ambient mantle conditions that best fit the 7 year post-Hector Mine cumulative displacements as well as the time series data. We use fits to the cumulative data to help eliminate models that do not lead to the correct pattern of surface deformation, as such rheologies cannot be made to fit the time series. Models that provide the best fit to time series data are found by adjusting d, β, and τ for diffusion creep models, and $\dot{\varepsilon}$, n, β, and τ for dislocation creep models. We considered all 55 stations shown in Figure 1 in the scoring of each model. For comparison to the cumulate displacements we only evaluate the model displacements after 7 years, while for the time series comparisons we consider the observations at 0.5 year intervals. A value of *wssr* less then ~1.7 is within the average 2σ uncertainty range of the functional representation of the time series and cumulative displacement. Our published uncertainty ranges for best fitting parameters provide the maximum range before the 2σ observational uncertainties are exceeded.

5. Results

5.1. Diffusion Creep Models

[26] We first consider steady state diffusion creep models to determine the range of ambient mantle conditions that are likely to produce well-fitting transient models. For steady state diffusion creep, viscosity is governed primarily by the geotherm and grain size. For each potential geotherm, we ran a suite of models with varying grain size, calculated postseismic surface displacements, and compared them to the observed 7 year cumulative displacements. We find that the best fitting hot geotherm model provides a significantly better solution (*wssr* = 1.5) than the best fitting models with either the median (*wssr* = 3.3) or cold (*wssr* = 4.4) geotherms (Figure 6a). These cooler geotherms lead to deeper flow, resulting in too broad a pattern of surface deformation. The better fit for the hot geotherm model indicates that postseismic flow is most vigorous in the relatively shallow portions of the mantle (50–70 km). Figure 6b shows that diffusion creep with a hot geotherm provides a reasonably

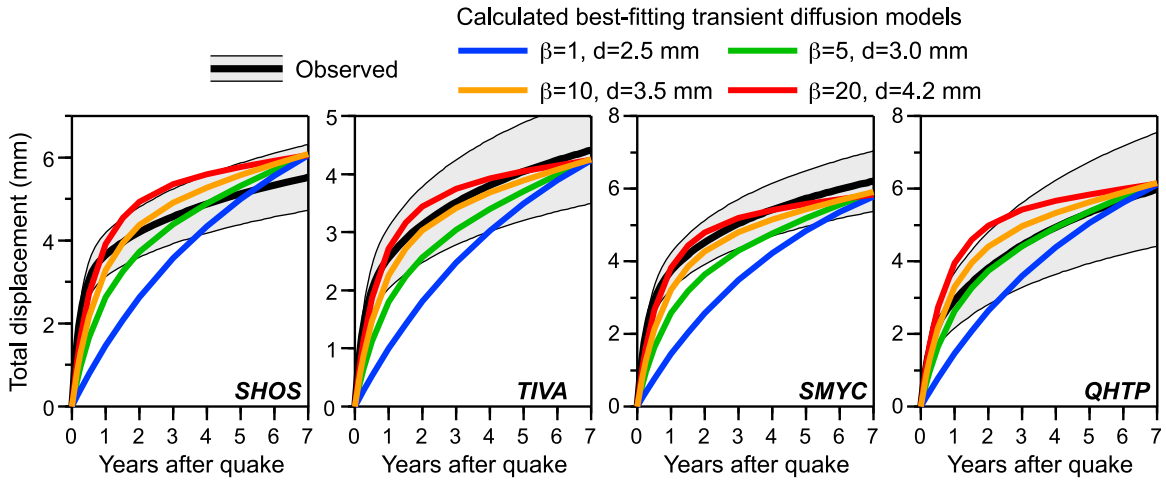

Figure 7. Comparison of the functional representation of observed displacement time series at four demonstrative GPS stations (see Figure 1 for locations) and those calculated based on the best fitting diffusion creep models as a function of the steady state to transient viscosity ratio, β. The grain size, d, is adjusted as noted in each model to enable a fit to the 7 year cumulative displacements. A hot geotherm (Figure 3) and a transient relaxation time, τ = 1 year is assumed in each model. Other diffusion parameters are as listed in Table 1.

good fit to the azimuth and magnitude of the far-field displacement field. The fit to the far-field azimuth data degrades significantly (up to 90°) for the models with cooler geotherms. Consideration of transient creep will not change this result, as the deformation pattern associated with diffusion creep is primarily controlled by the thermal gradient. Thus, we only consider hot geotherms in our exploration of transient diffusion rheologies.

[27] We explore transient diffusion creep models by varying β and τ and then solving for the grain size that leads to the minimum *wssr*. Figure 7 shows the observed and calculated time series at four representative GPS stations for models with varying β (β = 1 corresponds to the steady state rheology). We find a range of models that lead to surface deformation in reasonable agreement (*wssr* < 1.6) with the 7 year cumulative displacement. These models show the trade-off between variations in β and grain size; the rapid transient creep that occurs with large values of β is compensated by lower overall strain rates resulting from larger grain size.

[28] The best fitting transient diffusion creep models (*wssr* < 2.1 for time series fit) are characterized by $\beta \approx 10$–15, $\tau \approx 1.0 \pm 0.5$ years, and a grain size of d = 3.5 mm. Lower values of β underestimate early displacement rates, while higher values of β lead to an overshoot of the cumulative displacements at SHOS and QHTP once the transient creep rates slow after the first year. While not shown, lower values of τ do not provide sufficient time for high initial displacement rates to develop and higher values of τ lead to an overshoot of displacements after the first year. A value of $\beta \approx 10$ and is similar to values determined from the limited available laboratory data on the transient creep of olivine during diffusion creep [e.g., *Cooper*, 2002, Figure 6]. The applicability of these transient diffusion creep rheologies lies in the plausibility of the inferred grain size that is required to achieve the postseismic relaxation rates. This issue is addressed in the discussion below.

5.2. Dislocation Creep Models

[29] As with diffusion creep, we first use steady state flow models to assess the sensitivity of postseismic deformation to ambient mantle conditions. The three primary parameters that influence steady state dislocation creep are temperature, background strain rate, and the stress exponent. Lower viscosities are induced by higher temperatures, higher background strain rates, and lower stress exponents. Figure 8a shows the trade-off between the assumed thermal gradient and background mantle strain rate on the fit to 7 year cumulative displacements for n = 3.5 (laboratory average for wet olivine). The best fitting models are achieved with the hot and median geotherms (*wssr* = 1.9 and 2.0, respectively), with a modest degradation in fit for the cold geotherm (*wssr* = 2.4) due to azimuthal errors (Figure 8b). Further, these results show that the best fitting steady state models (with n = 3.5) all require a background strain rate greater than that observed at the surface (0.1 μstrain/yr). The required model strain rates can be diminished by including an initial transient phase in the models or by assuming a lower stress exponent.

[30] To explore the influence of transient creep, we investigate models assuming a thermal gradient, a mantle background strain rate, and a steady state to transient viscosity ratio, β, and then solve for the stress exponent and relaxation time that produce the best fitting displacement time series. We consider the three thermal gradients, five background mantle strain rates ($\dot{\varepsilon}$ = 0.02, 0.05, 0.10, 0.15, and 0.20 μstrain/yr), and five viscosity ratios (β = 1, 5, 10, 20, and 30), for a total of 75 baseline models. We evaluated models over a range of n = 3.2–3.8 and τ = 1–5 years.

[31] Figure 9a shows observed versus calculated time series at the same four representative GPS stations for models in which the viscosity ratio is varied (with the stress exponent tuned to the cumulative displacements for the prescribed choice of β). Each model assumes a hot geotherm, a background strain rate of 0.1 μstrain/yr (equal to the surface strain

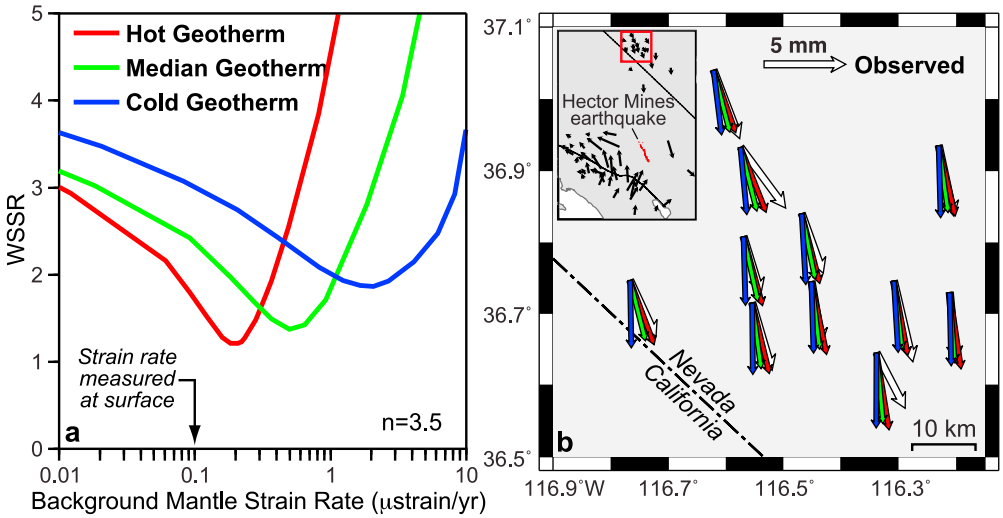

Figure 8. (a) Misfit (WSSR) of steady state dislocation creep models to 7 year cumulative displacements as a function of the assumed thermal gradient (Figure 3) and background mantle strain rate (other dislocation parameters as listed in Table 1). (b) Influence of the assumed thermal gradient on the azimuth of cumulative postseismic displacements for the best fitting steady state models for each assumed geotherm. Shown are stations in the far-field region 200 km to the north of the Hector Mine epicenter (see inset).

rate), and τ = 1 year. As with the diffusion creep models, lower values of τ do not provide sufficient time for high initial displacement rates to develop; higher values of τ lead to an overshoot of displacements after the first year (not shown). Results show that a value of $\beta \geq 10$ provides a reasonable fit to the observed time series (*wssr* < 1.9). While models with β values up to 30 provide a reasonable fit to the time series, laboratory data suggest a value of not more than 10. Models with lower values of β underpredict early fast displacement rates. Regardless of the assumed value of β, all of the models provide poorer fits to the time series data at station SHOS (left column of panels in Figure 9). Station SHOS has one of the most rapid changes in displacement rate versus time of all of the GPS stations, and was included in this demonstrative set of GPS stations to show one of the time series most difficult to replicate. At a 150 km from the Hector Mine epicenter, this station is located mid-range in comparison to the other stations (Figure 1), so this response is not a result of relative distance from the epicenter.

[32] Figure 9b shows observed versus calculated time series for models with different background strain rates and β = 10; the stress exponent was tuned to provide the best match to cumulative displacements. The observed time series are best fit for a background strain rate of $\dot{\varepsilon}$ = 0.1–0.2 μstrain/yr, which is comparable to the observed surface strain rate. Smaller background strain rates lead to insufficient displacements at the most distant stations (e.g., SMYC and TIVA in Figure 9b). This is because lower background strain rates lead to lower background stress levels, which in turn make the coseismic stress changes more significant compared to the total stress field. This effect focuses viscoelastic relaxation immediately beneath the fault, resulting in a shorter deformation wavelength and a poorer fit to the far-field displacement data.

[33] Figure 9c shows observed versus calculated time series for different thermal gradients with β = 10, τ = 1 year, and $\dot{\varepsilon}$ = 0.1 μstrain/yr). As with the steady state runs, the hot and median geotherms provide the best fitting models. This result implies that the greater depth of flow associated with the cold geotherm is not consistent with the data. In addition, the best fitting cold geotherm model requires a stress exponent of n = 3.18, which is at the lower end of the experimental uncertainty range. The median geotherm model requires a stress exponent of n = 3.24, while the hot geotherm requires n = 3.40, close to the median laboratory value.

[34] In summary, our best fitting dislocation creep model for wet olivine has a stress exponent of n = 3.40, a steady state to transient viscosity ratio of β = 10–15, a transient relaxation time of τ = 1 ± 0.5 year, with other flow-law parameters as indicated in Table 1. The best fits are achieved for the hot geotherm (Figure 3) and a background strain rate of 0.1 μstrain/yr. While our results do not rule out higher values for β, it is difficult to justify these based on the laboratory results.

6. Discussion

6.1. Assessing Diffusion Creep as the Controlling Mechanism

[35] Our best fitting models for transient diffusion creep require an olivine grain size of ~3.5 mm. We assess the viability of these models by considering whether a grain size of 3.5 mm would be stable within the implied mantle conditions. Grain size is controlled by the competition between static grain-growth and dynamic grain-size reduction [*Karato*, 1984]. *Austin and Evans* [2007] showed that grain size can be expressed as the balance of mechanical work between these two processes and that a steady state grain size, d_{ss}, can be derived for a set of mantle conditions (e.g., stress, strain rate, and temperature),

$$d_{ss} = \left(\frac{G_o e^{-(Q_g + PV_g)/RT} p_g^{-1} c\gamma}{\sigma \chi \dot{\varepsilon}_{disl}} \right)^{\frac{1}{1+pg}} \quad (10)$$

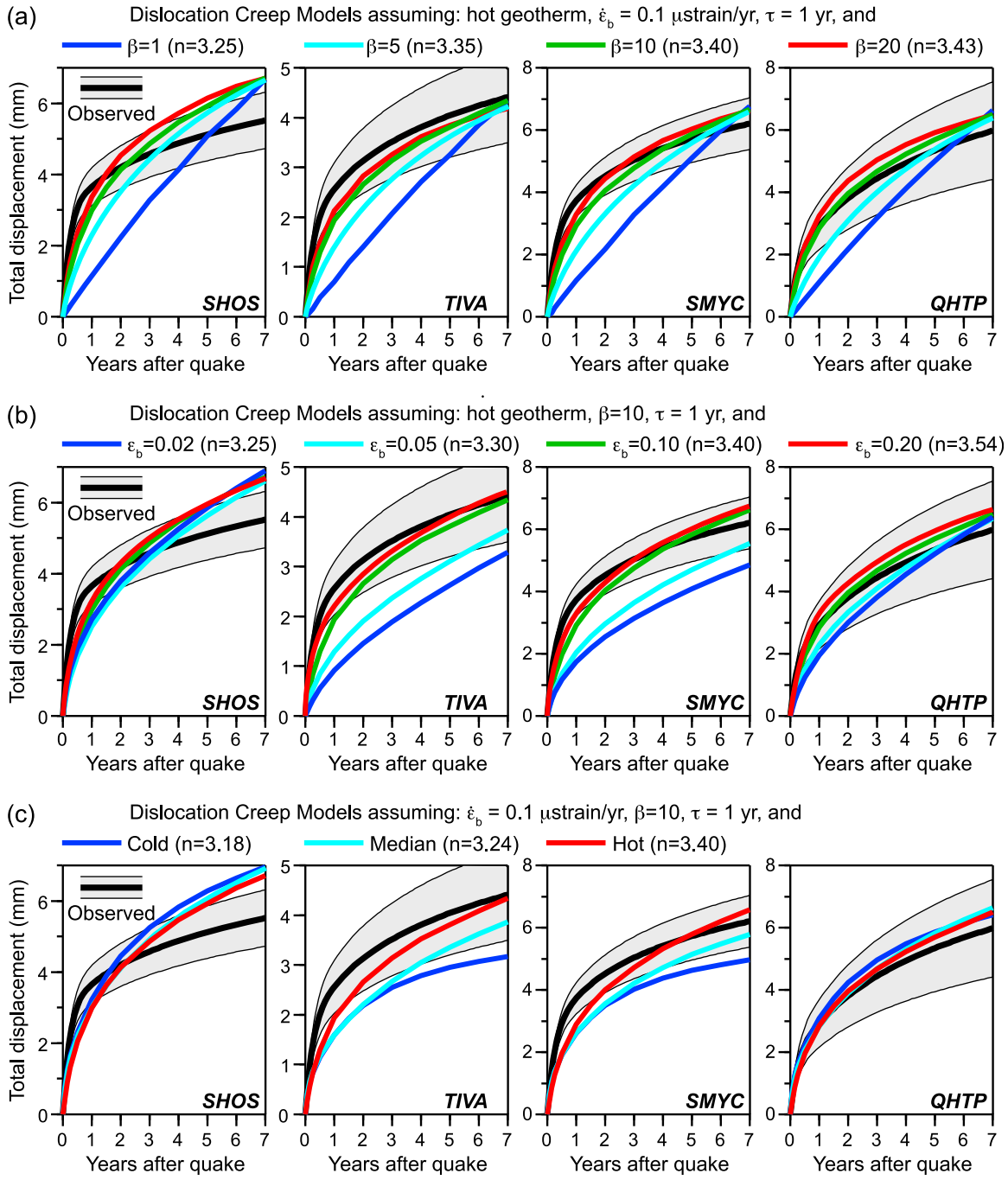

Figure 9. Comparison of the functional representation of observed displacement time series at four demonstrative GPS stations (see Figure 1 for locations) and those calculated based on the best fitting dislocation creep models as a function of the assumed (a) steady state to transient viscosity ratio, (b) background mantle strain rate, and (c) temperature gradient. The stress exponent of each model has been tuned to provide the best fit to the 7 year cumulative displacements for the set of model parameters described. Other dislocation parameters are as listed in Table 1.

where G_o is a grain growth rate constant, E_g and V_g are the activation enthalpy and volume for grain growth, p_g is an experimentally determined grain growth constant, γ is the average specific grain boundary energy, χ is the fraction of the work done by dislocation creep associated with changing grain boundary area, and c is a geometrical constant. Grain growth parameters for a diffusion creep of wet olivine are given in Table 2.

[36] To assess the best fitting diffusion creep models from this study, we examined mantle conditions at 60 km depth (~2 GPa), where postseismic flow is most vigorous. At this depth, the temperature of the hot geotherm is 1200–1300°C,

Table 2. Grain Size Evolution Parameters

Symbol	Description	Value	Units
d_{ss}	Steady state grain size		m
G_o	Grain growth rate constant for C_{OH} = 1000 H/10^6 Si	4.5×10^{-4}	m^{pg} s^{-1}
Q_g	Reference activation energy for grain growth	160	kJ/mol
V_g	Reference activation volume for grain growth	0	m^3/mol
p_g	Grain growth exponent	3	
γ	Average specific grain boundary energy	1	J/m^2
χ	Fraction of work done by dislocation creep to change grain boundary area	0.1	
c	Geometric constant	3	

and the steady state diffusion creep viscosity is $\sim 10^{19}$ Pa s. For a range of plausible background mantle strain rates ($\dot{\varepsilon}_b$ = 0.05–0.15 μstrain/yr based on the observed surface strain rate of 0.1 μstrain/yr [*Savage et al.*, 2003]) a viscosity of 10^{19} Pa s implies a background differential stress of 0.3–0.9 MPa.

[37] Evaluating equation (10) at these conditions results in a steady state grain size of 6–25 mm (intersection of horizontal gray band – defining a stress of 0.3 – 0.9 MPa, and the wattmeter curve in Figure 10), larger than the value of 3.5 mm required to explain the observed post-Hector Mine time series by diffusion creep. Extrapolation of lab-derived stress-grain size relationships results in an even larger grain size of 15–70 mm (labeled piezometer in Figure 10). To further illustrate the inconsistency of relatively small grain size with diffusion, we calculated a deformation mechanism map as a function of grain size and stress at 1200°C and C_{OH} = 1000 H/10^6Si (Figure 10). Figure 10 shows that for a grain size of 3.5 mm dislocation creep is the dominant deformation mechanism unless stresses are $<\sim$0.2 MPa; the stable grain size at 0.2 MPa is $\sim$100 mm based on the piezometer/wattmeter relationships. A stable grain size of 3.5 mm requires stresses in the range of 2 MPa and strain rates of $\sim$200 μstrain/yr, both of which are significantly higher than expected for the upper mantle (<1 MPa, <1 μstrain/yr). Moreover, at these conditions dislocation creep, not diffusion creep is the dominant deformation mechanism (Figure 10). For comparison, xenoliths from nearby regions of the Basin and Range and Colorado Plateau have grain sizes in the range of 1–20 mm [*Ave Lallemant et al.*, 1980; *Mercier*, 1980; *Wilshire*, 1990]. The grain size of the high-temperature (greater than 1050°C) xenoliths is around 5–20 mm, while the finer-grained samples often record lower lithospheric temperatures. Based on equation (10), a grain size of this magnitude is achieved at a strain rate of $\sim$0.5 μstrain/yr at the conditions illustrated in Figure 10. While this value is significantly larger than the

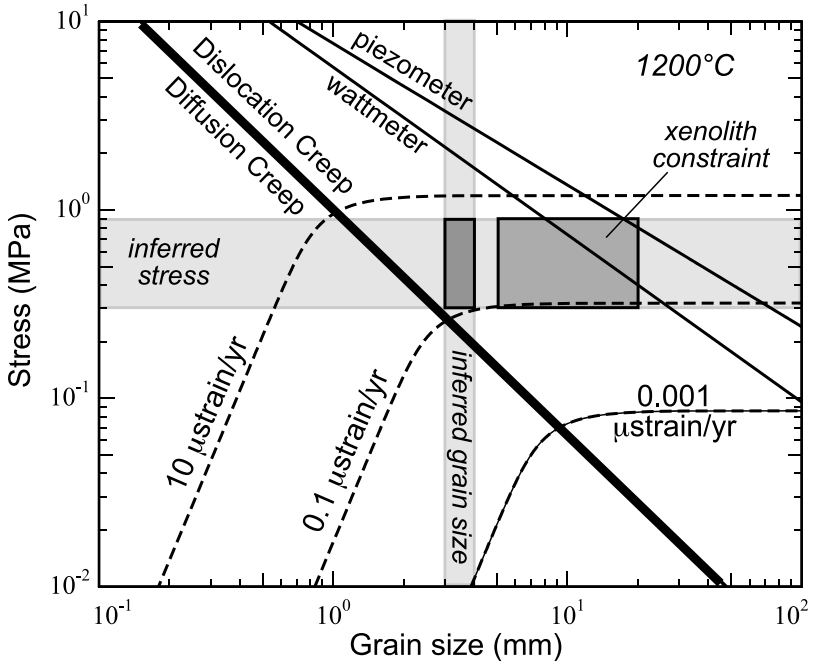

Figure 10. Deformation mechanism map for olivine calculated at 1200°C, 2 GPa, and C_{OH} = 1000 H/10^6 Si. Bold line illustrates the boundary between diffusion (left) and dislocation (right) creep. Constant strain rate contours (μstrain/yr) are shown by dashed black lines. The piezometer line shows extrapolation from the lab-based grain size piezometer of *Van der Wal et al.* [1993], the wattmeter line shows the steady state grain size calculated from equation (10) [*Austin and Evans*, 2007]. Vertical gray band illustrates best fitting grain size for the diffusion creep model shown in Figure 8. Horizontal gray band denotes stress range based on an average viscosity of 10^{19} Pa s and a range in strain rate from 0.05 to 0.15 μstrain/yr.

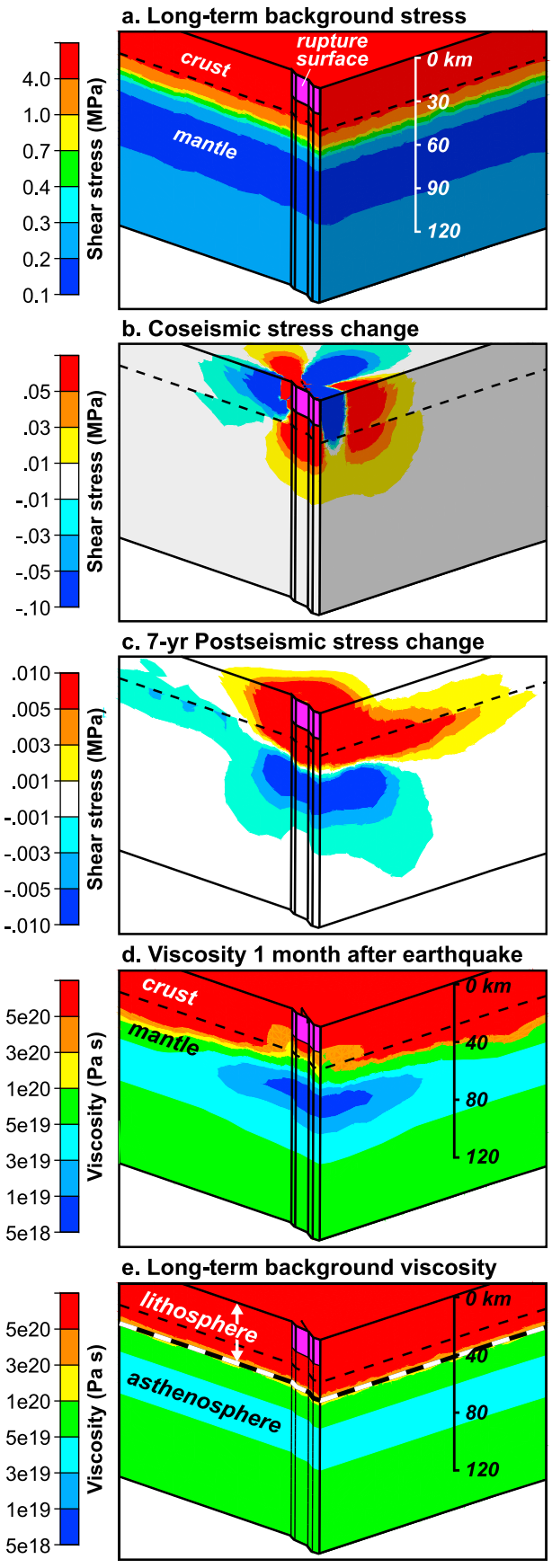

surface strain rate, asthenospheric flow resulting from the motion of the North American plate could result in laminar flow strain rates in this range. We conclude that a grain-size of 3.5 mm within shallow high-temperature mantle beneath the Mojave Desert is unlikely and diffusion creep is not the dominant mechanism responsible for postseismic flow in the mantle following the Hector Mine earthquake.

6.2. Implications for the Shallow Asthenosphere Through the Earthquake Cycle

[38] The best fitting dislocation creep model predicts a low viscosity region at relatively shallow depths (50–70 km) beneath southern California. We use the finite element model for this rheology and tectonic conditions (temperature and water content) to explore the stress state and viscosity structure at the base of the lithosphere through the earthquake cycle. Figure 11a shows the calculated long-term shear stress calculated for a regional strain rate of 0.1 μstrain/yr prior to both the Landers and Hector mine earthquakes. Shear stresses are calculated to be at least 4 MPa at the top of the mantle (30 km depth). Then, below a very thin mantle lid of only a few kilometers in thickness (consistent with seismic velocities [*Melbourne and Helmberger*, 2001]), shear stress decreases with depth to only 0.1–0.2 MPa at ~90 km depth, below which shear stress slowly increases due to the pressure dependence of viscosity The layer from 60 to 90 km depth, represent the weakest portion of the asthenosphere below southern California.

[39] Figure 11b shows the distribution of coseismic shear stress changes associated with the Hector Mine earthquake. Cool colors denote regions where shear stresses have been relieved by coseismic slip, while warm colors denote regions where slip led to an increase in shear stresses. Within the upper mantle, the Hector Mine earthquake increased shear stresses up to ~0.1 MPa immediately beneath the rupture. However, the mantle below a depth of ~60 km (top of the weakest layer) experienced shear stress changes of less than ~0.02 MPa. In both regions the induced stress changes are about an order of magnitude less than the background stress. Thus, the background stress, as opposed to the coseismic stress change, is the dominant component of stress influencing postseismic viscosities.

[40] Figure 11c shows the change in shear stress from just after the Hector Mine earthquake to 7 years after the

Figure 11. (a) Calculated long-term background shear stresses in the Eastern California Shear Zone (ECSZ) prior to the 1999 Hector Mine earthquake. Results are shown for the northern quadrant of the finite element model, with one face cutting through the Hector Mine rupture surface. (b, c) Calculated coseismic and postseismic shear stress changes, respectively. (d) Calculated viscosity structure of the ECSZ 1 month after the earthquake and (e) the long-term background viscosity structure. Results are shown for the best fitting model based on dislocation creep of wet olivine with a stress exponent of n = 3.40, a steady state to transient viscosity ratio of β = 10, a transient relaxation time of τ = 1 year, with the other flow-law parameters as indicated in Table 1, relaxing in a mantle environment with a hot geotherm (Figure 3) and a background strain rate of 0.1 μstrain/yr.

event (i.e., not including coseismic stress changes). These postseismic stress changes show a transfer of stress from the weak asthenosphere (below a depth of ~50 km) to the overlying lithosphere. This response illustrates how postseismic relaxation in the upper mantle can reload the rupture plane and increase shear stress in the surrounding region. These postseismic stress changes are relatively small, but may be sufficient to trigger critically loaded neighboring faults [e.g., *Freed and Lin*, 2001].

[41] Figures 11d and 11e show the inferred long-term background viscosity structure and the viscosity 1 month after the earthquake, respectively. These viscosity structures are determined based on the calculated stress and strain rate in these time periods (equation (5)). The background viscosity, which is a function of the background strain rate, is just above 5×10^{19} Pa s in the weak region below a depth of 50 km. Coseismic stress changes induce about an order of magnitude decrease in viscosity directly below the rupture plane. This reduction occurs primarily from transient creep, although there is a small contribution from the stress-dependence of the rheology. Thus, the drop in viscosity is short-lived, and returns to background conditions within the 7 year time span of this study, owing to the completion of the transient phase and the relaxation of coseismic stresses.

7. Conclusions

[42] We combined transient and steady state flow laws into a single constitutive relation that explains the response of a viscoelastic material to a change in stress based the ambient mantle conditions. This composite flow law allows us to use GPS displacement time series to infer the deformation environment within the upper mantle beneath the East California Shear Zone following the 1999 M7.1 Hector Mine earthquake. Specifically, we used a finite element model of the relaxation process constrained by surface displacement time series recorded by 55 continuous GPS stations for 7 years following the earthquake.

[43] Our results show that if postseismic relaxation was controlled by diffusion creep, it would require grain sizes of the order of 3.5 mm, a value considerably smaller than that expected based on laboratory-based grain size evolution models for corresponding upper mantle conditions (strain rate, temperature, pressure). By contrast, the observed postseismic response is well explained by dislocation creep occurring within a relatively hot upper mantle (e.g., 1200–1300°C at 50 km depth) assuming a long-term background mantle strain rate of ~0.1 μstrain/yr, consistent with the observed surface strain rate. Model results suggest that transient creep lasts ~1 year and occurs at viscosities ~10 times lower than subsequent steady state flow, in general agreement with laboratory observations. This short-lived, initial reduction in viscosity is the primary reason why the observed surface displacement rates decrease abruptly at the end of the first postseismic year. Our analysis would benefit from tighter constraints on transient behavior and grain size evolution from laboratory experiments during deformation in the dislocation creep regime.

[44] After achieving a reasonable fit to the GPS time series, we used our finite element model to explore the stress/viscosity of the upper mantle before and after the Hector Mine earthquake. The best fitting model shows that long-term background shear stresses at the top of the mantle are ~4 MPa, below which they decrease with depth to a minimum of 0.1–0.2 MPa at 70 km before increasing slowly with depth. This corresponds to a background viscosity of 10^{21} Pa s within a thin mantle lid that decreases to $\sim 5 \times 10^{19}$ Pa s within the underlying asthenosphere. The 1999 Hector Mine earthquake induced an immediate order of magnitude drop in viscosity within the upper mantle, associated with the transient rheology, which recovers to background levels within a few years. This study shows the utility of using short-term postseismic observations to infer long-term mantle conditions that are not readily observable by other means.

[45] **Acknowledgments.** This work was supported by the National Science Foundation grants EAR-0952234 (A.M.F.), EAR-0810188 (G.H.), and EAR-0854673 (M.D.B.). We would like to thank two anonymous reviewers for helpful suggestions that improved the manuscript.

References

Austin, N. J., and B. Evans (2007), Paleowattmeters: A scaling relation for dynamically recrystallized grain size, *Geology*, *35*, 343–346, doi:10.1130/G23244A.1.

Ave Lallemant, H. G., J.-C. C. Mercier, N. L. Carter, and J. V. Ross (1980), Rheology of the upper mantle: Inferences from peridotite xenoliths, *Tectonophysics*, *70*, 85–113, doi:10.1016/0040-1951(80)90022-0.

Behn, M. D., G. Hirth, and J. R. Elsenbeck II (2009), Implications of grain size evolution on the seismic structure of the oceanic upper mantle, *Earth Planet. Sci. Lett.*, *282*, 178–189, doi:10.1016/j.epsl.2009.03.014.

Bell, D. R., G. R. Rossman, J. Maldener, D. Endisch, and F. Rauch (2003), Hydroxide in olivine: A quantitative determination of the absolute amount and calibration of the IR spectrum, *J. Geophys. Res.*, *108*(B2), 2105, doi:10.1029/2001JB000679.

Borch, R. S., and H. W. Green II (1987), Dependence of creep in olivine on the homologous temperature and its implications for flow in the mantle, *Nature*, *330*, 345–348, doi:10.1038/330345a0.

Bürgmann, R., and G. Dresen (2008), Rheology of the lower crust and upper mantle: Evidence from rock mechanics, geodesy and field observations, *Annu. Rev. Earth Planet. Sci.*, *36*, 531–567, doi:10.1146/annurev.earth.36.031207.124326.

Carter, N. L., and H. G. Ave Lallemant (1970), High temperature flow of dunite and peridotite, *Geol. Soc. Am. Bull.*, *81*, 2181–2202, doi:10.1130/0016-7606(1970)81[2181:HTFODA]2.0.CO;2.

Carter, N. L., and S. Kirby (1978), Transient creep and semi-brittle behavior of crystalline rocks, *Pure Appl. Geophys.*, *116*, 807–839, doi:10.1007/BF00876540.

Carter, N. L., and M. C. Tsenn (1987), Flow properties of continental lithosphere, *Tectonophysics*, *136*, 27–63, doi:10.1016/0040-1951(87)90333-7.

Chopra, P. N. (1997), High-temperature transient creep in olivine rocks, *Tectonophysics*, *279*, 93–111, doi:10.1016/S0040-1951(97)00134-0.

Cooper, R. F. (2002), Seismic wave attenuation: Energy dissipation in viscoelastic crystalline solids, in *Plastic Deformation of Mineral and Rocks*, *Rev. Mineral. Geochem.*, vol. 51, edited by S. I. Karato and H. R. Wenk, pp. 253–290, Mineral. Soc. of Am., Washington, D. C., doi:10.2138/gsrmg.51.1.253.

Fialko, Y. (2004), Probing the mechanical properties of seismically active crust with space geodesy: Study of the coseismic deformation due to the 1992 M w 7.3 Landers (southern California) earthquake, *J. Geophys. Res.*, *109*, B03307, doi:10.1029/2003JB002756.

Freed, A. M. (2007), Afterslip (and only afterslip) following the 2004 Parkfield, California earthquake, *Geophys. Res. Lett.*, *34*, L06312, doi:10.1029/2006GL029155.

Freed, A. M., and R. Bürgmann (2004), Evidence of power-law flow in the Mojave Desert mantle, *Nature*, *430*, 548–551, doi:10.1038/nature02784.

Freed, A. M., and J. Lin (2001), Delayed triggering of the 1999 Hector Mine earthquake by viscoelastic stress transfer, *Nature*, *411*, 180–183, doi:10.1038/35075548.

Freed, A. M., R. Bürgmann, E. Calais, and J. Freymueller (2006), Stress-dependent power-law flow in the upper mantle following the 2002 Denali, Alaska, earthquake, *Earth Planet. Sci. Lett.*, *252*, 481–489, doi:10.1016/j.epsl.2006.10.011.

Freed, A. M., R. Bürgmann, and T. Herring (2007), Far-reaching transient motions after Mojave earthquakes require broad mantle flow

beneath a strong crust, *Geophys. Res. Lett.*, *34*, L19302, doi:10.1029/2007GL030959.

Freed, A. M., T. Herring, and R. Bürgmann (2010), Steady state laboratory flow laws alone fail to explain postseismic observations, *Earth Planet. Sci. Lett.*, *300*, 1–10, doi:10.1016/j.epsl.2010.10.005.

Gribb, T. T., and R. F. Cooper (1998), Low-frequency shear attenuation in polycrystalline olivine: Grain boundary diffusion and the physical significance of the Andrade model for viscoelastic rheology, *J. Geophys. Res.*, *103*, 27,267–27,279, doi:10.1029/98JB02786.

Gribb, T. T., and R. F. Cooper (2000), The effect of an equilibrated melt phase on the shear creep and attenuation behavior of polycrystalline olivine, *Geophys. Res. Lett.*, *27*, 2341–2344, doi:10.1029/2000GL011443.

Handy, M. R. (1990), The solid-state flow of polymineralic rocks, *J. Geophys. Res.*, *95*, 8647–8661, doi:10.1029/JB095iB06p08647.

Hearn, E. H., S. McClusky, R. Reilinger, and S. Ergintav (2005), Earthquake-cycle models as tie-breakers: Assessing candidate rheologies for ongoing Izmit earthquake postseismic deformation, *Eos Trans. AGU*, *87*(52), Fall Meet. Suppl., Abstract G32A-03.

Hearn, E. H., S. McClusky, S. Ergintav, and R. E. Reilinger (2009), Izmit earthquake postseismic deformation and dynamics of the North Anatolian Fault Zone, *J. Geophys. Res.*, *114*, B08405, doi:10.1029/2008JB006026.

Hirth, G., and D. L. Kohlstedt (2003), Rheology of the upper mantle and the mantle wedge: A view from the experimentalists, in *Inside the Subduction Factory*, *Geophys. Monogr. Ser.*, vol. 138, edited by J. Eiler, pp. 83–102, AGU, Washington, D. C.

Karato, S. (1984), Grain-size distribution and rheology of the upper mantle, *Tectonophysics*, *104*, 155–176, doi:10.1016/0040-1951(84)90108-2.

Karato, S. (2008), *Deformation of Earth Materials: An Introduction to the Rheology of Solid Earth*, 463 pp., Cambridge Univ. Press, Cambridge, U. K.

Karato, S., and P. Wu (1993), Rheology of the upper mantle: A synthesis, *Science*, *260*, 771–778, doi:10.1126/science.260.5109.771.

Kirby, S. H., and A. K. Kronenberg (1987), Rheology of the lithosphere; selected topics, *Rev. Geophys.*, *25*, 1219–1244, doi:10.1029/RG025i006p01219.

Korenaga, J., and S.-I. Karato (2008), A new analysis of experimental data on olivine rheology, *J. Geophys. Res.*, *113*, B02403, doi:10.1029/2007JB005100.

Lachenbruch, A. (1978), Heat flow in the Basin and Range province and thermal effects of tectonic extension, *Pure Appl. Geophys.*, *117*, 34–50, doi:10.1007/BF00879732.

Li, Z.-X. A., C.-T. A. Lee, A. H. Peslier, A. Lenardic, and S. J. Mackwell (2008), Water contents in mantle xenoliths from the Colorado Plateau and vicinity: Implications for the mantle rheology and hydration-induced thinning of continental lithosphere, *J. Geophys. Res.*, *113*, B09210, doi:10.1029/2007JB005540.

Mackwell, S. J., D. L. Kohlstedt, and M. S. Paterson (1985), The role of water in the deformation of olivine single crystals, *J. Geophys. Res.*, *90*, 11,319–11,334, doi:10.1029/JB090iB13p11319.

Mahsas, A., K. Yelles, K. Lammali, E. Calais, A. M. Freed, and P. Briole (2008), Shallow afterslip following the 2003 May 21, M_w=6.9 Boumerdes earthquake, Algeria, *Geophys. J. Int.*, *172*, 155–166, doi:10.1111/j.1365-246X.2007.03594.x.

Melbourne, T., and D. Helmberger (2001), Mantle control of plate boundary deformation, *Geophys. Res. Lett.*, *28*, 4003–4006, doi:10.1029/2001GL013167.

Mercier, J.-C. C. (1980), Magnitude of the continental lithospheric stresses inferred from rheomorphic petrology, *J. Geophys. Res.*, *85*, 6293–6303, doi:10.1029/JB085iB11p06293.

Polet, J., and H. Kanamori (2002), Anisotropy beneath California: Shear wave splitting measurements using a dense broadband array, *Geophys. J. Int.*, *149*, 313–327, doi:10.1046/j.1365-246X.2002.01630.x.

Pollitz, F. F. (2003), Transient rheology of the uppermost mantle beneath the Mojave Desert, California, *Earth Planet. Sci. Lett.*, *215*, 89–104, doi:10.1016/S0012-821X(03)00432-1.

Pollitz, F. F. (2005), Transient rheology of the upper mantle beneath central Alaska inferred from the crustal velocity field following the 2002 Denali earthquake, *J. Geophys. Res.*, *110*, B08407, doi:10.1029/2005JB003672.

Pollitz, F. F., and W. Thatcher (2010), On the resolution of shallow mantle viscosity structure using postearthquake relaxation data: Application to the 1999 Hector Mine, California, earthquake, *J. Geophys. Res.*, *115*, B10412, doi:10.1029/2010JB007405.

Post, R. L., Jr. (1977), High temperature creep of Mt. Burnet dunite, *Tectonophysics*, *42*, 75–110, doi:10.1016/0040-1951(77)90162-7.

Savage, J. C., J. L. Svarc, and W. H. Prescott (2003), Near-field postseismic deformation associated with the 1992 Landers and 1999 Hector Mine, California, earthquakes, *J. Geophys. Res.*, *108*(B9), 2432, doi:10.1029/2002JB002330.

Simons, M., Y. Fialko, and L. Rivera (2002), Coseismic deformation from the 1999 Mw 7.1 Hector Mine, California, earthquake as inferred from InSAR and GPS observations, *Bull. Seismol. Soc. Am.*, *92*, 1390–1402, doi:10.1785/0120000933.

Smith, B. K., and F. O. Carpenter (1987), Transient creep in orthosilicates, *Phys. Earth Planet. Inter.*, *49*, 314–324, doi:10.1016/0031-9201(87)90033-1.

Van der Wal, D., P. Chopra, M. Drury, and J. F. Gerald (1993), Relationships between dynamically recrystallized grain size and deformation conditions in experimentally deformed olivine rocks, *Geophys. Res. Lett.*, *20*, 1479–1482, doi:10.1029/93GL01382.

Wilshire, H. G. (1990), Lithology and evolution of the crust-mantle boundary region in the southwestern Basin and Range province, *J. Geophys. Res.*, *95*, 649–665, doi:10.1029/JB095iB01p00649.

Yang, Y., and D. W. Forsyth (2008), Attenuation in the upper mantle beneath Southern California: Physical state of the lithosphere and asthenosphere, *J. Geophys. Res.*, *113*, B03308, doi:10.1029/2007JB005118.

Zhao, Y.-H., S. B. Ginsberg, and D. L. Kohlstedt (2004), Solubility of hydrogen in olivine: Dependence on temperature and iron content, *Contrib. Mineral. Petrol.*, *147*, 155–161, doi:10.1007/s00410-003-0524-4.

M. D. Behn, Department of Geology and Geophysics, Woods Hole Oceanographic Institution, 360 Woods Hole Rd., MS 22, Woods Hole, MA 02543, USA.

A. M. Freed, Department of Earth and Atmospheric Sciences, Purdue University, 550 Stadium Mall Dr., West Lafayette, IN 47906, USA. (freed@purdue.edu)

G. Hirth, Geological Sciences, Brown University, Box 1846, 324 Brook St., Providence, RI 02912, USA.